

The article *Thermal Convection in Electrochemical Cells. Boundaries with Heterogeneous Thermal Conductivity and Implications for Scanning Electrochemical Microscopy* by Javor K. Novev and Richard G. Compton has been published in the journal *Physical Chemistry Chemical Physics* (DOI: 10.1039/C7CP01797A) and is available online at <http://pubs.rsc.org/en/content/articlelanding/2017/cp/c7cp01797a>.

PCCP

Accepted Manuscript

This article can be cited before page numbers have been issued, to do this please use: J. K. Novev and R. G. Compton, *Phys. Chem. Chem. Phys.*, 2017, DOI: 10.1039/C7CP01797A.



This is an Accepted Manuscript, which has been through the Royal Society of Chemistry peer review process and has been accepted for publication.

Accepted Manuscripts are published online shortly after acceptance, before technical editing, formatting and proof reading. Using this free service, authors can make their results available to the community, in citable form, before we publish the edited article. We will replace this Accepted Manuscript with the edited and formatted Advance Article as soon as it is available.

You can find more information about Accepted Manuscripts in the [author guidelines](#).

Please note that technical editing may introduce minor changes to the text and/or graphics, which may alter content. The journal's standard [Terms & Conditions](#) and the ethical guidelines, outlined in our [author and reviewer resource centre](#), still apply. In no event shall the Royal Society of Chemistry be held responsible for any errors or omissions in this Accepted Manuscript or any consequences arising from the use of any information it contains.

Thermal Convection in Electrochemical Cells. Boundaries with Heterogeneous Thermal Conductivity and Implications for Scanning Electrochemical Microscopy

Javor K. Novev and Richard G. Compton*

Department of Chemistry, Physical and Theoretical Chemistry Laboratory, Oxford University, South Parks Road, Oxford, OX1 3QZ, UK.

*Corresponding author. E-mail: Richard.Compton@chem.ox.ac.uk; Fax: +44 (0)1865 275 410; Tel: +44 (0)1865 275 957

Abstract: We investigate the heat transfer in a cylinder-shaped electrochemical cell with solid, thermally insulating walls. The cell is filled with a liquid and a solid substrate that is thermostated from below is situated at its base. The initial temperature of the liquid is different from that of the substrate so as to mimic imperfect thermostating in an electrochemical experiment; as heat transfer acts to diminish the temperature difference between the two, natural convection ensues. The influence of inhomogeneities in the thermal conductivity of the solid is studied – numerical simulations of the heat transfer in the system are conducted for substrates that are comprised of a thermally conductive material, an insulating one or a combination thereof. It is shown that the substrate structure strongly influences the structure and intensity of the natural convective flows emerging in the system. The present work demonstrates that under the idealized conditions under consideration, depending on the substrate structure, natural convection due to imperfect solution thermostating may give rise to flows whose local velocity can reach values as high as $10^{-3} \text{ m}\cdot\text{s}^{-1}$. Moreover, as comparison between cells of two different radii shows, both the intensity and the temporal evolution of the flows arising in this system are highly sensitive to the precise geometry of the experimental cell. These results can have far-reaching consequences for the interpretation of results from experimental techniques such as scanning electrochemical microscopy.

I. Introduction

The understanding of electrochemical systems requires an appreciation of the interplay of a diversity of physical phenomena including electron transfer, mass transport, chemical reactions, adsorption/desorption processes, etc., all of which are temperature-sensitive. Accordingly, for decades it has been a *sine qua non* that investigations of electrical interfaces are conducted under conditions of effective thermostating to ensure a known and uniform temperature throughout the system under study. That this is achieved is important because of the strong temperature dependence of quantities

determined via electrochemical techniques, e.g. rate constants (both homogeneous and interfacial), diffusion coefficients and equilibrium constants. Moreover, it is very frequently the case that electrochemical experiments are interpreted and modelled on the basis of the assumption that the transport of reactants, intermediates and products in the vicinity of the electrode|solution interface occurs exclusively via diffusion and sometimes electromigration. The latter can only be true if the cell temperature is uniform – should there be a temperature gradient, this could drive a natural convective flux, which could contribute significantly to the measured electrical current.

We have recently shown that the enthalpy change associated with electrode processes is, for typical reactions under conventional measurement conditions, insufficient to induce a convective flow of magnitude sufficient to perturb the electrochemical process or preclude its interpretation in terms of diffusion-only transport¹, the reason being that heat dissipation, for example in aqueous media, occurs orders of magnitude faster than diffusional mass transport. Nonetheless, as we have also shown¹⁻², the occurrence of an electrochemical reaction can lead to non-negligible convective mass currents driven by concentration gradients. Furthermore, on the basis of detailed simulation, we have recently concluded that the rigorous thermostating of electrochemical cells is mandatory if convection is to be rigorously excluded³. Thus, if the cell contents are at a different temperature to their surroundings at the onset of the experiment, the analysis of data from the latter on the assumption of diffusion-only transport may be compromised. That said, for many years the vital importance of temperature control in electrochemical systems has been recognised and measures have been taken to implement it⁴.

One widely-used technique electrochemical experiment, dating back now more than two decades⁵⁻⁷, in which effective thermostating is difficult and rarely performed, is the so-called scanning electrochemical microscopy (SECM). In this experiment, a microelectrode is rastered across a solid|liquid interface of interest, electrochemical or otherwise, and a faradaic current is measured at the microelectrode surface as a function of the microelectrode position. Thus currents measured at constant electrode-substrate separation are used to 'image' the surface of the former whilst 'approach curves' are used to obtain quantitative information of different types. All of this presumes an absence of convection which might either 'smear' or fully obscure an image or invalidate quantitative analyses made on the basis of diffusion-only models. Our previous work demonstrates the role of imperfect thermostating in promoting natural convection in a model SECM cell³. There, we assumed that the lower boundary of the cell was perfectly thermally insulating. Experimentally, it is often the case that the lower boundary of the cell is the substrate whose structure is of interest in SECM, see e.g. Schäfer et al.⁸ Examples include the study of electron-transfer reactions at non-uniform surfaces, for instance at boron-doped diamond (BDD) electrodes⁹ and also for graphitic surfaces where the contributions of basal plane and edge plane components of the surface have been known to show contrasting electron transfer kinetics since the pioneering work of McCreery and co-workers¹⁰⁻¹².

In the present paper, we explore the role of substrate composition in heat transfer within a model electrochemical cell and its influence on *local* convection under conditions of imperfect thermostating. Specifically, we consider a surface composed of zones of different but isotropic thermal conductivity. Such substrates occur in experimental practice – examples include particle/polymer composites where metal surfaces are surrounded by poor conductors and electrodes embedded in an insulator. A similar situation can also arise for instance in the case of non-monocrystalline graphitic substrates as the thermal conductivity of graphite is strongly anisotropic – at 300 K, the thermal conductivity in the direction of the basal plane is reported to be between 100 and 1000 times greater than in the orthogonal direction¹³⁻¹⁴.

II. Theoretical model

Here, we describe the theoretical basis of our simulations of convective heat and momentum transfer in electrochemical cells with inhomogeneous substrates.

As in our previous paper on thermal convection in SECM³, we consider a solution whose temperature is initially uniform but different from that of its surroundings. Heat transfer with the environment leads to local variations in temperature and density, which in turn lead to buoyancy forces within the fluid. The substrate temperature is initially also homogeneous, and its value at the lower substrate surface is held constant by a thermostat throughout the simulated experiment. This configuration conceptually resembles the experimental setup of Schäfer et al.⁸, although in their case heat is supplied in pulses.

In contrast to our previous work on SECM, we do not account for the heat transfer in the solid cell and the surrounding air. Instead, we model a highly idealized cylindrical cell that has solid, thermally insulated top and side walls and deal only with the heat transfer within the solution and the substrate. Furthermore, we assume that the problem is axisymmetric and therefore that all quantities are independent of the polar angle ϕ . We make these considerable simplifications in order to isolate and maximize the effect under study, namely, the influence of non-uniformities in the substrate's thermal conductivity on the predicted convective patterns. We should, however, point out that this limits our current work to a 'proof-of-concept' study as, for example, the substitution of the free solution|air boundary with a solid one alters the velocity distribution in the liquid phase. As stated, the problem deals with a form of Rayleigh-Bénard convection, a phenomenon that has been studied in the literature most extensively for the flow between infinite horizontal planes¹⁵, but the case of cylindrical enclosures has also been covered¹⁶; as we will observe, heat transfer induces circulatory convective motion in the fluid.

We consider two different idealized models for the electrochemical cell, both of them approximating it as a thermally insulated cylinder with solid walls, radius r_{cell} and height h_{cell} situated on top of a cylindrical substrate of height h_s and radius r_{cell} ; the

coordinate origin is at the centre of the substrate's lower surface, as illustrated in Figure 1. The first model accurately reflects the typical radius of the aperture containing the substrate in a typical SECM measurement cell, $r_{\text{cell}} = 3$ mm (CH Instruments, Inc., Austin, TX, USA, <http://www.chinstruments.com>, see our previous paper³ for an illustration). Thus, the substrate radius corresponds to the maximum substrate size that could be studied experimentally in this cell. In the second model, we set the radius of the solid container and the substrate to be equal to that of the wider part of the cell, that is, 8 mm. The height of the cell is the same for both models and for the second one ensures that the volume of liquid within the cylinder corresponds to that in the typical SECM experiment. As we will show below, the cell dimensions strongly affect both the intensity and the evolution of the convective flows generated by the initial temperature difference, which reinforces our point on the importance of rigorous thermostating in electrochemical experiments.

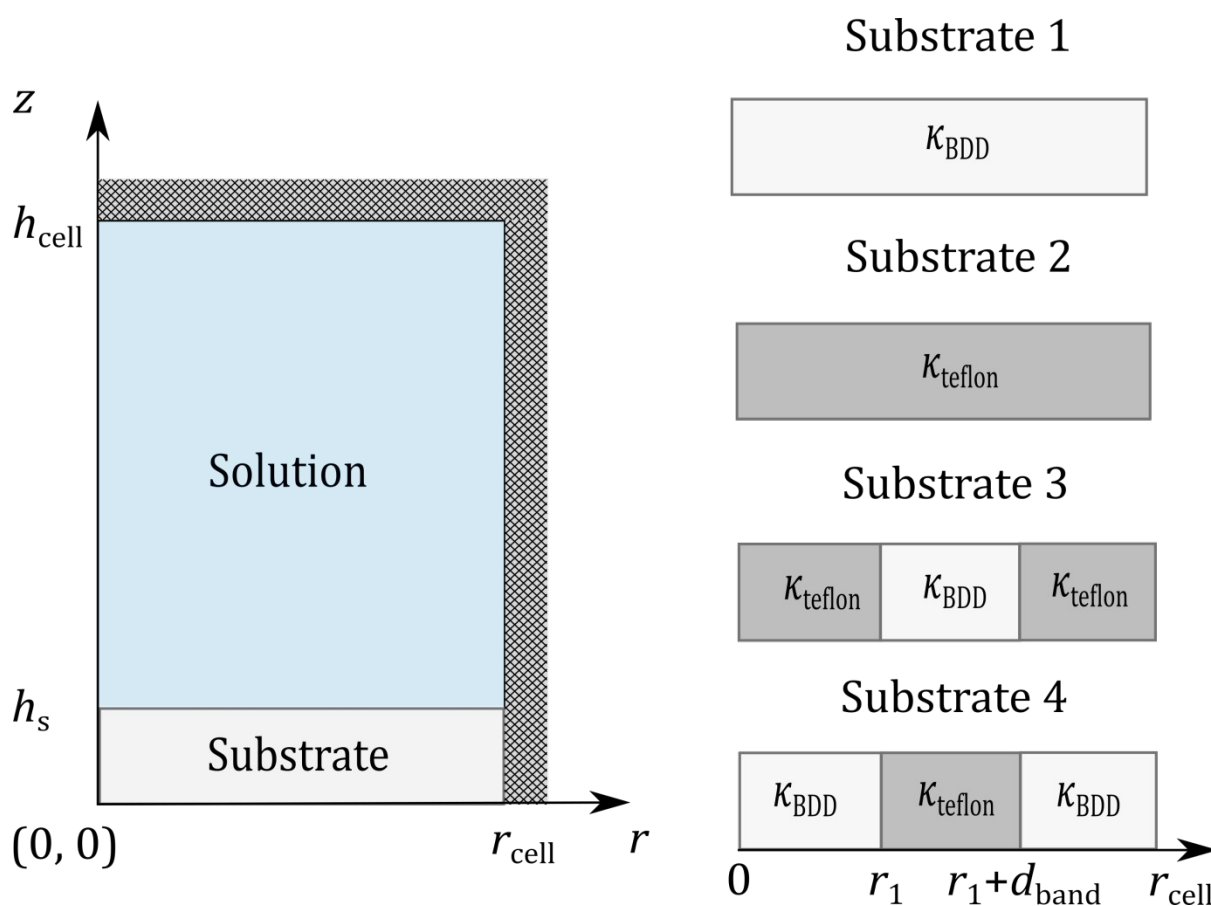


Figure 1. Geometry of the model we use for the measurement cell and structure of the studied substrates – 1) homogeneous BDD cylinder; 2) homogeneous tefflon cylinder; 3) tefflon cylinder with a BDD annular band; 4) BDD cylinder with a tefflon annular band. We presume that the temperature and velocity distributions are axially symmetric and we therefore only have to simulate the region pictured in the figure.

We explore several different cases for the solid substrate at the bottom of the cell. Our study deals with homogeneous substrates comprised of either BDD or polytetrafluoroethylene (tefflon), which differ markedly in their thermal conductivity κ_i , as well as substrates comprised mainly of one of these materials with an embedded annular band of the other that has a width of d_{band} and is situated between $r_1 = (r_{\text{cell}} -$

$d_{\text{band}})/2$ and $r_1 + d_{\text{band}}$, see Section III for details. Among these configurations, the one with a ring of BDD embedded in teflon is particularly relevant experimentally, as it can serve as a model for an annular band electrode. Natural convection coupled with heat transfer in a solid body has been studied before in the literature, for example Kaminski and Prakash¹⁷ have analysed numerically the effect of conduction in one of the vertical walls of a square enclosure, Saeid¹⁸ has dealt with a similar problem for a two-dimensional porous enclosure via simulations, and Kim and Viskanta¹⁹ have studied natural convection in a square cavity with conducting walls through both simulations and experiments.

The temperature profile in the solution follows a convective heat equation of the form

$$\frac{\partial T^L}{\partial t} + \mathbf{v} \cdot \nabla T^L = \chi^L \nabla^2 T^L, \quad (1)$$

where t is time, χ^L – is the thermal diffusivity [$\text{m}^2 \cdot \text{s}^{-1}$] of the liquid, \mathbf{v} is its velocity determined from the Navier-Stokes equation and T^L is its temperature.

In the solid phase, the temperature is influenced only by heat conduction, and obeys a simpler form of the heat equation,

$$\frac{\partial T^S}{\partial t} = \chi^S \nabla^2 T^S, \quad (2)$$

where χ^S and T^S are the thermal diffusivity and the temperature of the substrate. Throughout the text, we will use the symbol T to refer to the temperature profile in the whole system, i.e., to T^L and T^S collectively.

Initially, the temperature of the substrate is homogeneous,

$$T^S|_{t=0} = T_{\text{thermostat}}. \quad (3)$$

The temperature of the substrate's bottom surface is maintained constant throughout the simulated experiment

$$T^S|_{z=0} = T_{\text{thermostat}}, \quad (4)$$

in practice this may be achieved by having a thermostat at the plane $z = 0$.

At the start of the studied process, the temperature of the solution is uniform but different from that of the substrate,

$$T^L|_{t=0} = T_{\text{thermostat}} - \Delta T, \quad (5)$$

where the initial temperature difference ΔT can be either positive or negative.

Rather than considering the heat transfer through the walls of the cell as in our previous paper on the subject³, we model the boundaries of the cell as thermally insulating,

$$\left. \frac{\partial T^L}{\partial r} \right|_{r=r_{\text{cell}}} = 0; \quad (6)$$

$$\left. \frac{\partial T^L}{\partial z} \right|_{z=h_s+h_{\text{cell}}} = 0, \quad (7)$$

View Article Online
DOI: 10.1039/C7CP01797A

In reality, as our previous simulations indicate³, there can be a substantial heat flux through the side walls of the cell; however, we choose to neglect it here in the interest of simplicity and in order to highlight the qualitative local effects of the inhomogeneities in the substrate thermal conductivity.

Likewise, we assume there is no radial heat flux through the boundary of the substrate,

$$\left. \frac{\partial T^S}{\partial r} \right|_{r=r_{\text{cell}}} = 0. \quad (8)$$

At the interface between the substrate and the solution, both the temperature and the heat flux need to be continuous²⁰,

$$(T^L - T^S)|_{z=h_s} = 0; \quad (9)$$

$$(\kappa^L T^L - \kappa^S T^S)|_{z=h_s} = 0, \quad (10)$$

where $\kappa^i = \rho_i \cdot C_{p,i} \cdot \chi^i$ is the thermal conductivity [$\text{W} \cdot \text{m}^{-1} \cdot \text{K}^{-1}$] of the respective medium, ρ_i - its density, and $C_{p,i}$ - its heat capacity at constant pressure.

The solid substrate plays a key role in our present study, and we will study several different configurations for its structure. In the simplest case, we take the substrate to be homogeneous and consisting either of boron-doped diamond or of teflon. However, the main focus of our study is on inhomogeneous substrates; the inhomogeneity considered is an annular band of conductivity κ_{band} and thickness d_{band} situated between a disc of radius $r_1 = (r_{\text{cell}} - d_{\text{band}})/2$ and an outer band of radius r_{cell} , both of them with conductivity κ_0 :

$$\kappa = \begin{cases} \kappa_0, & r < r_1 \\ \kappa_{\text{band}}, & r_1 < r < r_1 + d_{\text{band}} \\ \kappa_0, & r_1 + d_{\text{band}} < r < r_{\text{cell}} \end{cases} \quad (11)$$

The substrate's other properties, such as its density and heat capacity, follow analogous distributions. For substrates with annular bands, the solid temperature and the heat flux obey conditions analogous to eqs. (9)-(10) at the boundaries between the two materials, situated at $r = r_1$ and $r = r_1 + d_{\text{band}}$.

We now turn to the hydrodynamic problem. We assume that the fluid is incompressible and Newtonian; therefore, the velocity field is controlled by the Navier-Stokes equation²¹, for which we use the approximate form

$$\rho_0 \left(\frac{\partial \mathbf{v}}{\partial t} + \mathbf{v} \cdot \nabla \mathbf{v} \right) = -\nabla \Delta p + \eta \nabla^2 \mathbf{v} - \rho_0 \alpha (T^L - T^L|_{t=0}) \mathbf{g}, \quad (12)$$

where η is the solution viscosity and α - its thermal expansion coefficient at constant pressure, $\alpha = -1/\rho(\partial\rho/\partial T)_p$, $\mathbf{g} = -|\mathbf{g}|\mathbf{e}_z = -9.81\text{m} \cdot \text{s}^{-2} \mathbf{e}_z$ is the gravitational acceleration vector, and Δp is defined as the difference between the pressure at a given time and the initial value,

$$\Delta p = p - p_0 + \rho_0 z |g|, \quad (13)$$

with p_0 being the pressure $z = 0$ at the start of the simulated experiment.

We solve the Navier-Stokes equation in conjunction with the continuity equation

$$\nabla \cdot \mathbf{v} = 0. \quad (14)$$

As in our previous papers¹⁻³, we adopt the Boussinesq approximation of the governing equations (1), (12) and (14) – namely, we linearize the fluid density with respect to temperature and treat all of its other properties as constant. Furthermore, within this standard approach, we only consider the temperature-dependence of density in the buoyancy force term and not in the continuity equation (14) – see e.g. Kundu and Cohen for a justification²¹.

In line with our aim to simplify the model as much as possible, we apply no-slip conditions to the boundaries of the cell, which is equivalent to treating all of them as solid,

$$\mathbf{v}|_{r=r_{\text{cell}}, h_s < z < h_{\text{cell}} + h_s} = \mathbf{v}|_{0 < r < r_{\text{cell}}, z = h_{\text{cell}} + h_s} = \mathbf{v}|_{0 < r < r_{\text{cell}}, z = h_s} = \mathbf{0}. \quad (15)$$

The boundary conditions (6)-(7) for the heat flux and (15) for the velocity mean that in our model, the solution is enclosed in a solid, thermally insulating cell. Let us note once more that, in reality, SECM measurement cells are open to the surrounding air (see e.g. Chapter 2 in the book on SECM edited by Bard and Mirkin²²) and heat transfer through the solution|air interface and the side walls of the cell plays a role³.

At the beginning of the simulated experiment, the solution under study is stagnant,

$$\mathbf{v}|_{t=0} = \mathbf{0}. \quad (16)$$

Utilizing the assumed symmetry of the problem, we seek a numerical solution of the equations (1) and (12) only in a rectangular region of dimensions r_{cell} by $h_{\text{cell}} + h_s$ (pictured in Figure 1). For that reason, we impose additional boundary conditions at the symmetry axis, $r = 0$. For the temperature profiles, the symmetry condition requires that there is no radial flux at $r = 0$,

$$\left. \frac{\partial T^L}{\partial r} \right|_{r=0} = 0; \quad (17)$$

$$\left. \frac{\partial T^S}{\partial r} \right|_{r=0} = 0. \quad (18)$$

From symmetry considerations, the radial velocity at the cylinder axis is subject to the constraints²⁶

$$v_r|_{r=0} = 0; \quad (19)$$

$$\left. \frac{\partial v_z}{\partial r} \right|_{r=0} = 0. \quad (20)$$

Note that the continuity conditions (9)-(10) at the interfaces and the symmetry conditions (17)-(20) are implicitly handled by the COMSOL Multiphysics²³ modules for Heat Transfer in Fluids and Laminar Flow applied to systems with axial symmetry.

In our previous papers on natural convection in electrochemistry^{1,3}, we stated that we also use the boundary condition $\partial v_r / \partial z|_{r=0} = 0$. While this equation is fulfilled both in the simulations in Refs.^{1,3} and those we discuss here, it cannot be regarded as a separate boundary condition because it follows directly from eq. (19).

Further, we note that our assumption for axial symmetry of the flows is not necessarily fulfilled – previous studies, notably that by Neumann²⁴, who performed three-dimensional simulations, indicate that axisymmetric flows in related systems are inherently unstable and more complex flow patterns are realized instead. On the other hand, Torrance and Rockett²⁵ have experimentally observed axisymmetric flows for another similar system. Thus, it is difficult to make a prediction regarding the symmetry of the flows for our specific case. In this study we assume that the flows are axially symmetric; a more rigorous approach would involve performing three-dimensional simulations or gathering experimental data to test this assumption.

We can gain some insight into the parameters that control the flow of the solution by introducing the dimensionless variables

$$\begin{aligned} \tilde{r} &= \frac{r}{h_{\text{cell}}}; \tilde{z} = \frac{z}{h_{\text{cell}}}; \tilde{\mathbf{v}} = \frac{h_{\text{cell}}}{\chi^L} \mathbf{v}; \tilde{p} = \frac{h_{\text{cell}}^2}{\rho_0 (\chi^L)^2} \Delta p; \tilde{t} = \frac{\chi^L}{h_{\text{cell}}^2} t; \\ \tilde{T} &= \frac{T^L - T^L|_{t=0}}{T_{\text{thermostat}} - T^L|_{t=0}} = \frac{T^L - T^L|_{t=0}}{\Delta T}, \end{aligned} \quad (21)$$

as well as the Rayleigh and Prandtl numbers,

$$Ra = \frac{\rho_0 \alpha h_{\text{cell}}^3 |\Delta T| |g|}{\chi^L \eta} \quad \text{and} \quad (22)$$

$$Pr = \frac{\eta}{\rho_0 \chi^L}. \quad (23)$$

The governing equations for the fluid phase therefore assume the form²⁴:

$$\tilde{\nabla} \cdot \tilde{\mathbf{v}} = 0; \quad (24)$$

$$\partial_{\tilde{t}} \tilde{\mathbf{v}} + \tilde{\mathbf{v}} \cdot \tilde{\nabla} \tilde{\mathbf{v}} = -\tilde{\nabla} \tilde{p} + Pr \tilde{\nabla}^2 \tilde{\mathbf{v}} + Ra Pr \text{sgn}(\Delta T) \tilde{T} \mathbf{e}_z; \quad (25)$$

$$\partial_{\tilde{t}} \tilde{T} + \tilde{\mathbf{v}} \cdot \tilde{\nabla} \tilde{T} = \tilde{\nabla}^2 \tilde{T}, \quad (26)$$

where $\text{sgn}(x)$ refers to the sign function. Thus, the heat and mass transport in the system are controlled by Ra and Pr . We study a particular cell of height h_{cell} and conduct all our calculations for water, taking its properties to be constant and equal to their values at the initial temperature. Hence, the only parameter that we can vary to modify the behaviour of the system is the initial temperature difference ΔT ; its value is particularly important because in problems of the type studied, natural convection becomes significant and starts to influence the heat transfer once the Rayleigh number exceeds a certain critical value, Ra_{cr} .

Note that the dimensionless temperature \tilde{T} is defined so that it tends to unity as t approaches infinity – at equilibrium, $T^L = T_{\text{thermostat}}$ – and the force term becomes constant and can no longer drive convective motion. More precisely, the order of

magnitude for the characteristic time required for \tilde{T} to reach unity is the same as for one-dimensional heat conduction, $\tau = h_{\text{cell}}^2/\chi^L \sim 10^2$ s, in contrast with our previous results for a cell of the same dimensions, where $\tau \sim 10^3$ s³. This difference comes from the fact that in our current study, a thermostat at the bottom of the cell serves as a heat source or sink, depending on the sign of ΔT , whereas in our previous model this role is performed by the air at a finite but large distance from the cell and heat is lost or gained through the side walls of the electrochemical cell.

Studies of problems similar to ours but possessing a constant driving force for the convection, e.g. those by Yamaguchi et al.²⁶, have examined the dependence of the critical Rayleigh number on the cylinder aspect ratio ($r_{\text{cell}}/h_{\text{cell}}$). Moreover, as discussed by Yamaguchi et al.²⁶, in principle there are infinitely many possible modes of flow consisting of multiple convective rolls, each of them having a different critical Ra . The complexity of the flow patterns that can arise in systems like the one under consideration here is a strong argument for the importance of eliminating natural convection as a factor in electrochemical experiments. The sensitivity of the flows to the parameters of the system, particularly the aspect ratio ($r_{\text{cell}}/h_{\text{cell}}$), makes accounting for the convective contribution to the electrical currents measured in those experiments a daunting task.

III. Simulations

This section deals with the implementation of our simulations and discusses our choice of parameters.

We have simulated a substrate of height $h_s = 1$ mm and cells of height $h_{\text{cell}} = 7$ mm and radius $r_{\text{cell}} = 3$ mm and 8 mm, as discussed above.

The properties of the solution were approximated with those of water at either 293.15 K or 303.15 K, i.e., at the initial temperature $T^L(t=0) = T_\infty - \Delta T$ corresponding to $\Delta T = 5$ K and $\Delta T = -5$ K, respectively. The values $\alpha = 2.06 \times 10^{-4}$ K⁻¹ for the thermal expansion coefficient, $\eta = 1.002$ mPa·s for the viscosity, $\kappa^L = 0.5984$ W·m⁻¹·K⁻¹ for the thermal conductivity, $\rho_0 = 998.21$ kg·m⁻³ for the density and $C_p^L = 4.1818 \times 10^3$ J·kg⁻¹·K⁻¹ for the heat capacity were used at $T^L(t=0) = 293.15$ K, whereas at $T^L(t=0) = 303.15$ K, the calculations were done with $\alpha = 3.02 \times 10^{-4}$ K⁻¹, $\eta = 0.7977$ mPa·s, $\kappa^L = 0.6154$ W·m⁻¹·K⁻¹, $\rho_0 = 995.65$ kg·m⁻³ and $C_p^L = 4.1784 \times 10^3$ J·kg⁻¹·K⁻¹; all values were taken from the CRC Handbook of Chemistry and Physics¹⁴.

The parameters of water at 303.15 K were also used for all simulations with varying negative ΔT conducted for $r_{\text{cell}} = 3$ mm to establish approximate bounds for Ra_{cr} ; similarly, for the simulations with $\Delta T > 0$, the properties of water were taken at 293.15 K. As our approximate model is most appropriate for small $|\Delta T|$, we have only performed simulations with $|\Delta T| = 3, 4$ and 5 K; initial temperature differences larger

than 5 K in absolute value are also less likely to arise in the experiment. The parameters we use correspond to Prandtl numbers $Pr = 5.4$ at negative and 7.0 at positive ΔT , and to Rayleigh numbers in the range between $Ra = 2.6 \times 10^4$ and 4.3×10^4 and 1.4×10^4 and 2.4×10^4 , respectively.

As we have stated above, we consider substrates comprised of BDD, teflon or an annular band of one material embedded within a cylinder of the other one (see Figure 1). For annular bands, the material properties of the solid follow an equation of the form (11). For cells of radius 3 mm, we have simulated substrates with three different thicknesses of the annular band - $d_{\text{band}}/r_{\text{cell}} = 1/3$, $1/9$ and $1/27$, whereas for $r_{\text{cell}} = 8$ mm, we have only considered $d_{\text{band}}/r_{\text{cell}} = 1/3$.

For the density and heat capacity of substrates of high thermal conductivity, we use the values for non-doped diamond at 298.15 K from the CRC Handbook¹⁴, $\rho_{\text{diamond}} = 3513 \text{ kg}\cdot\text{m}^{-3}$, $C_{p, \text{diamond}} = 508.33 \text{ J}\cdot\text{mol}^{-1}\cdot\text{K}^{-1}$; we take its thermal conductivity to be $\kappa_{\text{BDD}} = 1600 \text{ W}\cdot\text{m}^{-1}\cdot\text{K}^{-1}$, as reported for BDD by Prikhodko et al.²⁷

The thermally insulating substrate in our model is polytetrafluoroethylene (teflon); its density is²⁸ $\rho_{\text{teflon}} = 2200 \text{ kg}\cdot\text{m}^{-3}$, its thermal conductivity²⁹ - $\kappa_{\text{teflon}} = 0.26 \text{ W}\cdot\text{m}^{-1}\cdot\text{K}^{-1}$. We should point out that in our previous paper on the subject³, we used the same value of κ_{teflon} , citing a study by Price and Jarratt³⁰ that refers to 323.15 K; however, given the weak temperature dependence of κ_{teflon} ²⁹, this has very little effect the accuracy of our calculations. For the heat capacity of teflon, we take the value for the crystalline form measured at 298.15 by Lau et al.³¹ - $C_{p, \text{teflon}} = 898.1 \text{ J}\cdot\text{mol}^{-1}\cdot\text{K}^{-1}$; note that for the amorphous form the value would be $1025.5 \text{ J}\cdot\text{mol}^{-1}\cdot\text{K}^{-1}$.

The governing equations (1)-(2), (12) and (14) were solved numerically via the finite element method in the commercial software package COMSOL Multiphysics 5.2²³. Linear shape functions were used for the velocity components, the pressure and the temperature profiles in most simulations. In several cases, noted below, quadratic shape functions were used for the temperature.

Unless otherwise noted, the simulated experiments were with a duration of 600 s, which is the typical time scale for reaching thermal equilibrium in the studied systems.

For comparison, simulations with no account for convection were also performed. In them, we only solved eqs. (1)-(2) with the fluid velocity set to zero; the settings for the mesh and the time stepping were identical to those for the simulations involving convection, with the exception that only linear elements were used for T .

IV. Results and discussion

In this section, we discuss the properties of the natural convective flows for the various substrate structures under study.

For the purpose of analysing the different cases, we define the volume-averaged velocity and temperature, which give a measure of the overall motion and heat transfer within the liquid,

$$|\mathbf{v}_{\text{av}}| = \frac{1}{V} \int_V \sqrt{v_r^2 + v_z^2} dV \quad \text{and} \quad (27)$$

$$\Delta T_{\text{av}} = \left| \frac{\int_V (T^L - T^L(t=0)) dV}{\int_V (T^L(t=0) - T_{\text{thermostat}}) dV} \right| = \frac{1}{\pi r_{\text{cell}}^2 h_{\text{cell}}} \frac{1}{\Delta T} \int_V (T^L - T^L(t=0)) dV, \quad (28)$$

where V denotes the volume of the liquid in the cell. At long t , as the system tends towards equilibrium, the temperature throughout the system becomes homogeneous and equal to that of the thermostat, therefore at this limit, the value of ΔT_{av} is unity.

Below, we illustrate the development of the convective flows on the scale of the whole cell through plots of the dependence of $|\mathbf{v}_{\text{av}}|$ on time. In all studied cases, the solution is stagnant at $t = 0$, see eq. (16), and, after passing through one or several extrema, its average velocity approaches zero at long t . The reason for this characteristic dependence of $|\mathbf{v}_{\text{av}}(t)|$ is that the driving force for convective motion, the temperature difference between the thermostat and the solution, diminishes with time, and eventually reaches zero at equilibrium. Alongside the plots of $|\mathbf{v}_{\text{av}}(t)|$, we also present ‘snapshots’ of the temperature and velocity profiles that illustrate the local properties of the distributions at some of the extrema in $|\mathbf{v}_{\text{av}}(t)|$.

In all studied systems, we are chiefly concerned with the semi-quantitative description of the system and, most importantly, the order of magnitude of the velocity fields that natural convection generates. For that reason, instead of discussing all details of the evolution of the convective flows, we will only focus on its main stages.

IV. 1. Simulations for $r_{\text{cell}} = 3 \text{ mm}$

First, we give a detailed account of the simpler flows that arise within a cylindrical cell whose radius corresponds to the maximum substrate radius that can fit in a standard cell for SECM (CH Instruments).

1. A. Solution colder than substrate at $t = 0$ ($\Delta T > 0$)

In this configuration, the fluid is being heated from below, which causes the fluid layers in contact with the substrate to expand and rise upwards, thereby enhancing the heat transfer.

Homogeneous BDD substrate

For a homogeneous BDD substrate, we observe two qualitatively different types of flow, depending on the order of the shape function employed for T . Both patterns consist in a single toroidal roll, but are set apart by the direction of the fluid motion within it –

linear elements lead to clockwise motion in the simulated region, whereas quadratic give rise to a flow of the opposite direction. This is discussed below.

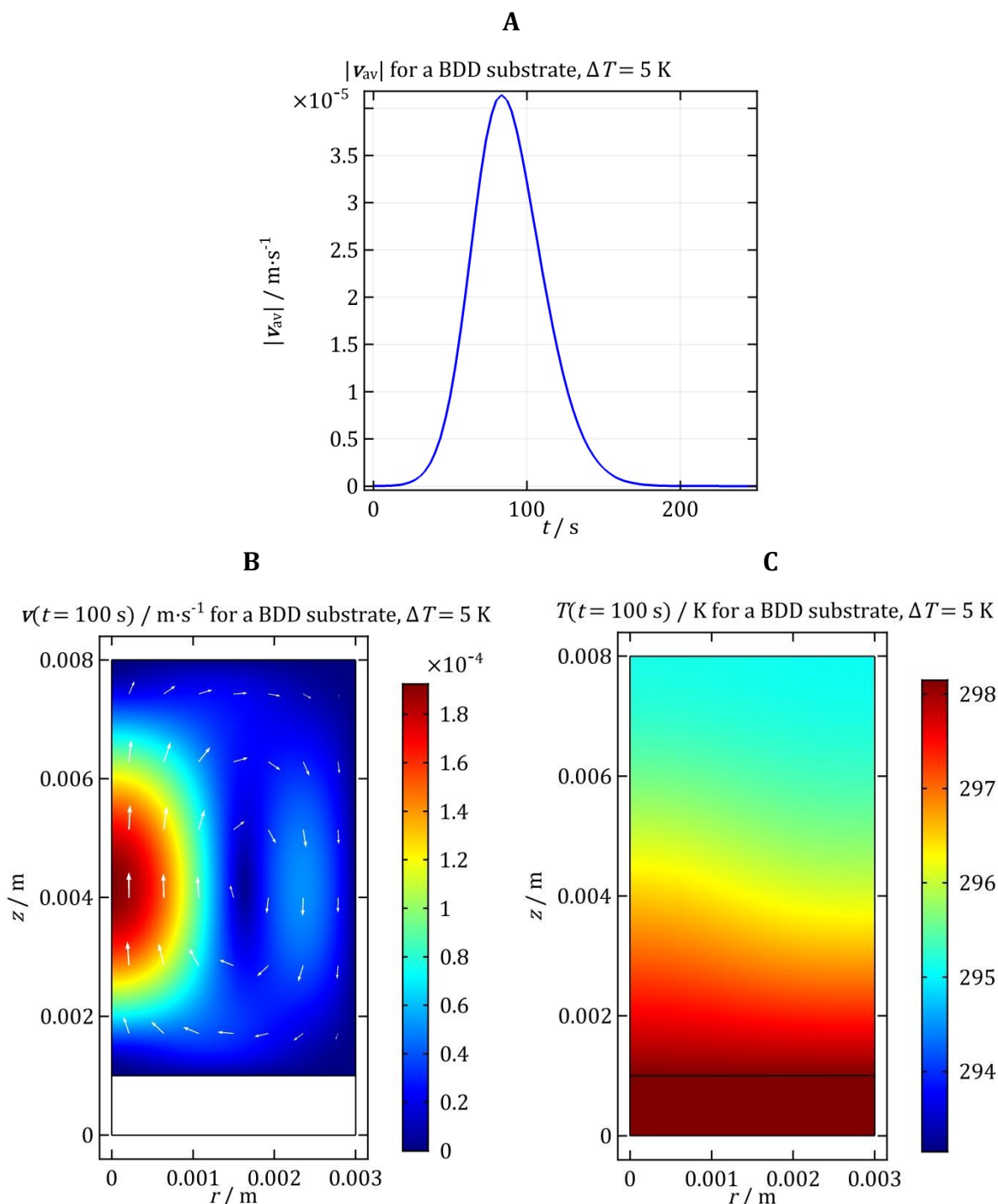


Figure 2. Results for a homogeneous BDD substrate obtained from a simulation that uses linear elements for T : **A** – volume-averaged velocity magnitude vs. time; **B** and **C** – ‘snapshots’ respectively of \mathbf{v} and T at $t = 100$ s. The length of the arrows in **B** is proportional to natural logarithm of the absolute value of the velocity at the given point. For this simulation, the solution is colder by $\Delta T = 5$ K than the substrate at the initial moment.

The two flows differ in their intensity – whereas the clockwise flow pattern exhibits local velocities as high as $|\mathbf{v}_{local}| \sim 10^{-4} \text{ m} \cdot \text{s}^{-1}$ and $|\mathbf{v}_{av}| \sim 10^{-5} \text{ m} \cdot \text{s}^{-1}$ (see Figure 2A-B), for the anticlockwise one, $|\mathbf{v}_{local}| \sim 10^{-6} \text{ m} \cdot \text{s}^{-1}$ and $|\mathbf{v}_{av}| \sim 10^{-7} \text{ m} \cdot \text{s}^{-1}$ (Figure 2A and Figure S2B in the Supplementary information). This difference is easily understandable in

intuitive terms – from the symmetry condition (20) and the no-slip condition at the cylinder side wall, it follows that $|v_z|$ has an extremum at $r = 0$. As in this case there is heating from below and the buoyancy force has a positive z -component, the fluid can be expected to have a positive vertical velocity at $r = 0$, thus giving a clockwise flow pattern in the simulated region. For an anticlockwise pattern to be established, the liquid at $r = 0$ needs to move downwards against the buoyancy force, which explains the reduced magnitude of its velocity.

The temperature distributions corresponding to the two flows are also markedly different – whereas the clockwise flow perturbs T significantly and gives rise to a distribution that has a maximum at $r = 0$ (Figure 2C), in the other case, T depends only weakly on the radial coordinate (Figure S2D). Note that on the scale of the whole cell, neither type of flow affects the temperature distribution strongly – the difference in ΔT_{av} with respect to the conduction-only case is at most $\sim 1\%$ for the clockwise flow and significantly less for the anticlockwise one, see Figure S1 and Figure S2B in the Supplementary information. As even at $|\Delta T| = 5$ K the effect on temperature is so small, we do not attempt to establish bounds for Ra_{cr} for a homogeneous BDD substrate.

It is not surprising that we obtain more than one solution to the same problem in view of the fact that the Navier-Stokes equation (12) is nonlinear – the system permits the existence of multiple solutions – flows with upwelling either at the centre or at the side walls of a cylindrical container have been reported by Yamaguchi et al.²⁶, Müller et al.³² and Tuihri et al.¹⁶ for similar configurations. If multiple solutions exist, however, they need not be of the same stability. We should also note that if the Rayleigh number is increased significantly beyond the values we consider in this work, flows of greater complexity will arise, for example consisting of multiple rolls lined up in the radial or the normal direction, as previous studies report^{26,16}.

As a qualitative way of assessing the stability of the two types of solutions we observed, we modified the boundary condition at the top cylinder wall to

$$T^L|_{z=h_{cell}+h_s} = T_{\text{thermostat}} - \Delta T, \quad (29)$$

so that the driving force of the convective flow does not go to zero as t tends to infinity and there is a stationary state with a non-zero velocity. At the steady state, we observed the same two types of flow we discussed above, but in contrast to the time-dependent case, the velocity magnitudes were nearly identical. To assess the relative stability of the clockwise and anticlockwise flow, we used the stationary distributions of T , \mathbf{v} and p from the simulation that yielded one type of pattern as an initial condition for the other one; for all simulations of BDD substrates, the flow direction remained unchanged. Furthermore, the stationary flow patterns obtained from simulations with an initially stagnant solution were preserved upon reverting from eq. (29) back to a no-flux boundary condition.

These results imply that the velocity distributions in Figure 2 and Figure S2 are manifestations of two equally stable flow patterns that can be obtained from one

another via reflection with respect to the plane $z = h_s$. The reason for the higher intensity of the clockwise flow, is that in it, the fluid at the cylinder axis, which has the highest velocity magnitude, moves upwards, i.e., in the direction of the buoyancy force. For the anticlockwise flow, the velocity at $r = 0$ is negative and the fluid has to move against the buoyancy force, which results in a reduced velocity magnitude. A reduced velocity magnitude in turn means that convective heat transfer is less efficient in this case, which is why we observe that the temperature profile (Figure S2C) is approximately independent of r , indicating that heat is transported exclusively by conduction. The difference with T from Figure 2 is due to the different temporal evolution of \mathbf{v} in this problem; were the driving force to remain independent of time the temperature distributions corresponding to both flow types would become distorted to the same degree, as we have shown in the Supplementary Information (Figure S3C and Figure S4C).

While we obtain dissimilar types of flow depending on the specific discretization scheme that we use, we only observe such a difference for systems that involve homogeneous substrates. Our qualitative stability tests indicate that in this case alone, there exist two similarly stable flow patterns of equivalent stability. Given that the initial state is unstable, in principle an infinitesimal variation in the initial conditions may cause the system to enter either of them and which is realized is likely determined by small numerical inaccuracies in the discretization. Below, we show that, for substrates with annular bands, the direction of flow plays a role in the stability of the convective patterns and that for the presently discussed value of r_{cell} , a single one is consistently obtained regardless of the discretization. The likely reason is that for inhomogeneous substrates, the variations in temperature induced by the substrate inhomogeneity are sufficient to make one or the other direction of flow preferable.

Homogeneous teflon substrate

In contrast to BDD, teflon is a thermal insulator ($\kappa_{\text{teflon}}/\kappa_{\text{BDD}} \sim 10^{-4}$), leading to a much lower heat flux through the solid. For that reason, in a system with a teflon substrate, heat conduction through the liquid is fast enough to prevent the build-up of strong perturbations in the density near the substrate-solution interface, which in turn leads to negligible velocities ($|\mathbf{v}_{\text{av}}| \lesssim 10^{-8} \text{ m}\cdot\text{s}^{-1}$). Accordingly, the temperature in the fluid remains essentially unperturbed by the flow and independent of r , see the Supplementary information for details.

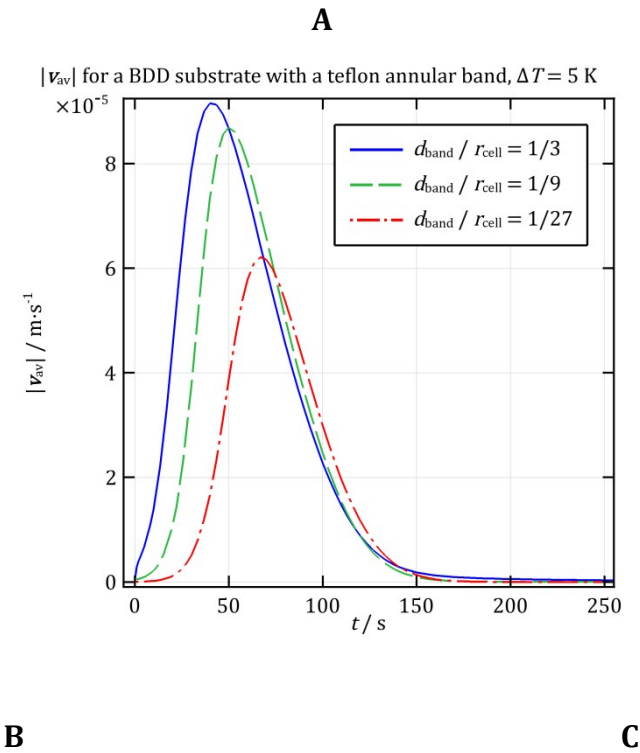
BDD substrates with teflon annular bands

Convective flows consisting of a single toroidal roll with anticlockwise motion in the simulated region (i.e., upwelling next to the wall) arise in the simulations of conducting substrates with an insulating annular band. Accordingly, the solution temperature reaches its maximum value along r at the side wall and has a minimum at the centre of the cylinder. As Figure 3A illustrates, the maximum volume-averaged velocity $|\mathbf{v}_{\text{av}}|_{\text{max}}$ for this case ($6 \text{ to } 9 \times 10^{-5} \text{ m}\cdot\text{s}^{-1}$) is higher than in the clockwise flow observed for a

homogeneous BDD substrate ($3.5 \times 10^{-5} \text{ m}\cdot\text{s}^{-1}$, Figure 2A), but has the same order of magnitude.

The properties of the flow for this case are markedly dependent upon the substrate structure – increasing the width of the insulating band leads to an increase in both $|\mathbf{v}_{\text{av}}|_{\text{max}}$ and the induction time for establishing the convective flow. The explanation behind this is that a substrate with a wider band causes a stronger perturbation in the liquid temperature at $z \sim h_s$ (compare Figure 3C with Figure S8B and D). The temperature within the conducting region remains homogeneous and approximately equal to that of the thermostat. In contrast, as seen in Figure 3C, the insulating region cools down noticeably because heat is lost to the liquid at a higher rate than it is gained from the thermostat at $z = 0$. The width of the annular band affects the extent of the perturbation and whereas for small d_{band} it is effectively smoothed out by the heat transfer in the liquid, for the larger values it perturbs the density distribution considerably and leads to the quicker establishment of a convective flow pattern. In the Supplementary information, we provide ‘snapshots’ of the temperature and velocity distribution for $d_{\text{band}}/r_{\text{cell}} = 1/9$ and $1/27$, which complement those presented in Figure 3 for $d_{\text{band}}/r_{\text{cell}} = 1/3$.

By running additional simulations with $\Delta T = 3$ and 4 K and examining $\Delta T_{\text{av}}(t)$, we established that the critical value of the initial temperature difference lies between 4 and 5 K, corresponding to the range between 1.9×10^4 and 2.4×10^4 for Ra_{cr} . The comparison between the results for $\Delta T_{\text{av}}(t)$ at different ΔT and simulations with no convection is shown in Figure S9 in the Supplementary information.



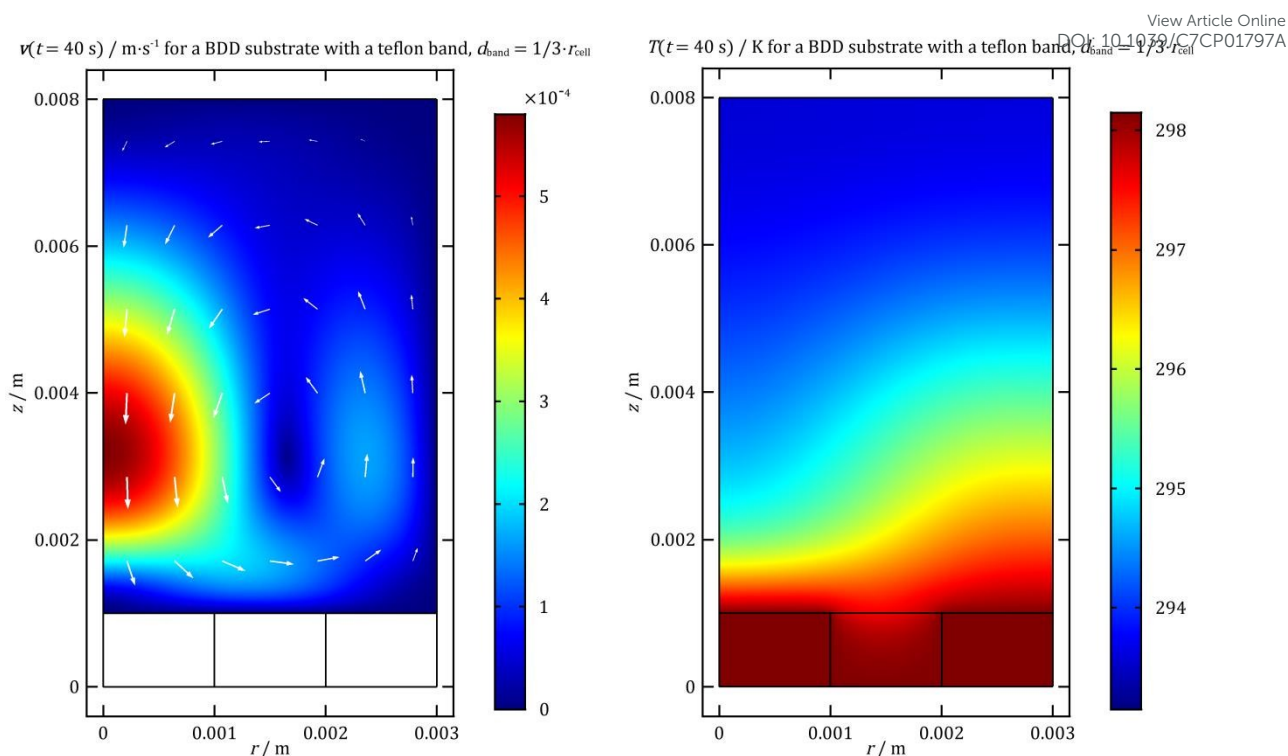


Figure 3. Results for BDD substrates with teflon annular bands. **A** – volume-averaged velocity magnitude vs. time; **B** and **C** – ‘snapshots’ respectively of \mathbf{v} and T at $t = 40$ s for a band with $d_{\text{band}}/r_{\text{cell}} = 1/3$. The length of the arrows in **B** is proportional to natural logarithm of the absolute value of the velocity at the given point. For this simulation, the solution is colder by $\Delta T = 5$ K than the substrate at the initial moment.

Our tests using the alternate boundary condition (29) indicate that the flow with upwelling at $r = 0$ is of equivalent stability to the one shown in Figure 3 under conditions that admit a stationary state with non-zero velocity. However, starting from the stationary distributions of \mathbf{v} , T and p obtained in this configuration and changing the boundary condition at the top wall back to no-flux, we see that for this substrate structure, only the pattern with downward motion at $r = 0$ is stable under transient conditions; for more details on the stability tests, see the Supplementary Information. At a qualitative level, the preferred direction of flow is due to the presence of a conductive outer band, which leads to a higher T^{L} in the vicinity of the side wall than next to the insulating band. Even though the same is true for the inner band, as it is in contact with a much smaller amount of liquid, the perturbation at $r \sim r_{\text{cell}}$ is the determining factor and causes the fluid to move upwards next to the wall.

Teflon substrates with BDD annular bands

Single toroidal rolls with upwelling in the centre of the cylinder and temperature profiles that have a maximum at the axis except in the vicinity of the thermally insulating substrate are observed for this case, contrasting with the results for BDD substrates with teflon annular bands. The average velocity is $|\mathbf{v}_{\text{av}}| \sim 10^{-4} \text{ m}\cdot\text{s}^{-1}$ – compare with the case for a homogeneous teflon substrate, in which $|\mathbf{v}_{\text{av}}| \lesssim 10^{-8} \text{ m}\cdot\text{s}^{-1}$, see Figure S6A-Figure S7A in the Supplementary Information.

A

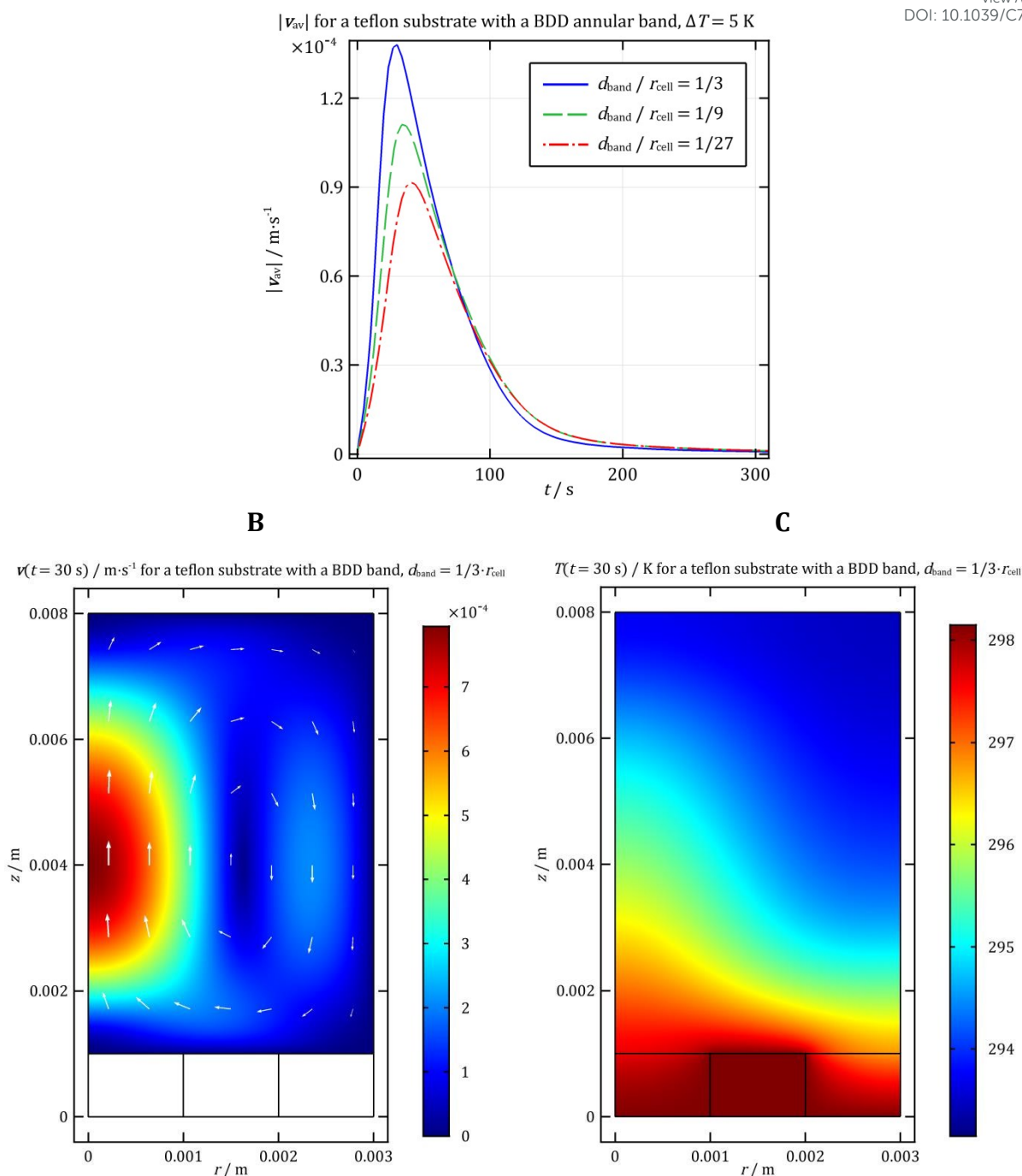


Figure 4. Results for teflon substrates with BDD annular bands. **A** – volume-averaged velocity magnitude vs. time; **B** and **C** – ‘snapshots’ respectively of \mathbf{v} and T at $t = 30$ s for a band with $d_{\text{band}}/r_{\text{cell}} = 1/3$. The length of the arrows in **B** is proportional to natural logarithm of the absolute value of the velocity at the given point. For this simulation, the solution is colder by $\Delta T = 5$ K than the substrate at the initial moment.

By analogy with the ‘inverse’ configuration, we performed studies at varying ΔT with the aim of establishing bounds for Ra_{cr} . Again as with the case of a BDD substrate with a teflon annular band, we observe that convection only starts to have an appreciable influence over ΔT_{av} when the initial temperature difference is increased from 3 K to 4 K, and that this is caused by a substantial increase in the peak average velocity, as illustrated in Figure 5 for $d_{\text{band}}/r_{\text{cell}} = 1/3$ (see Figure S14-Figure S15 for

details on the other studied substrates). Thus, we obtain that for this case, Ra_c is between 1.4×10^4 and 1.9×10^4 .

As with the ‘inverse’ configuration, increasing the band width intensifies the convective flow due to the stronger perturbation of the temperature profile at $z \sim h_s$. The induction time for the onset of convection decreases as d_{band} is increased (Figure 4A), but the dependence is much weaker than for a conducting substrate with an insulating annular band, compare with Figure 3A. Another similarity with the case of a conducting substrate with an insulating band is that the flow shown in Figure 4 and its approximate mirror image with respect to $z = h_s$ are approximately equivalent in stability in systems that permit a stationary flow, but not if the driving force for convection decays to zero at long t . At a qualitative level, the difference in flow direction with the ‘inverse’ case comes from the absence of a strong positive perturbation in T^L at $r \sim r_{\text{cell}}$. Without this factor, the fluid follows the direction of the buoyancy force at $r = 0$, leading to a normal velocity profile that exhibits a maximum rather than a minimum at the cylinder axis.

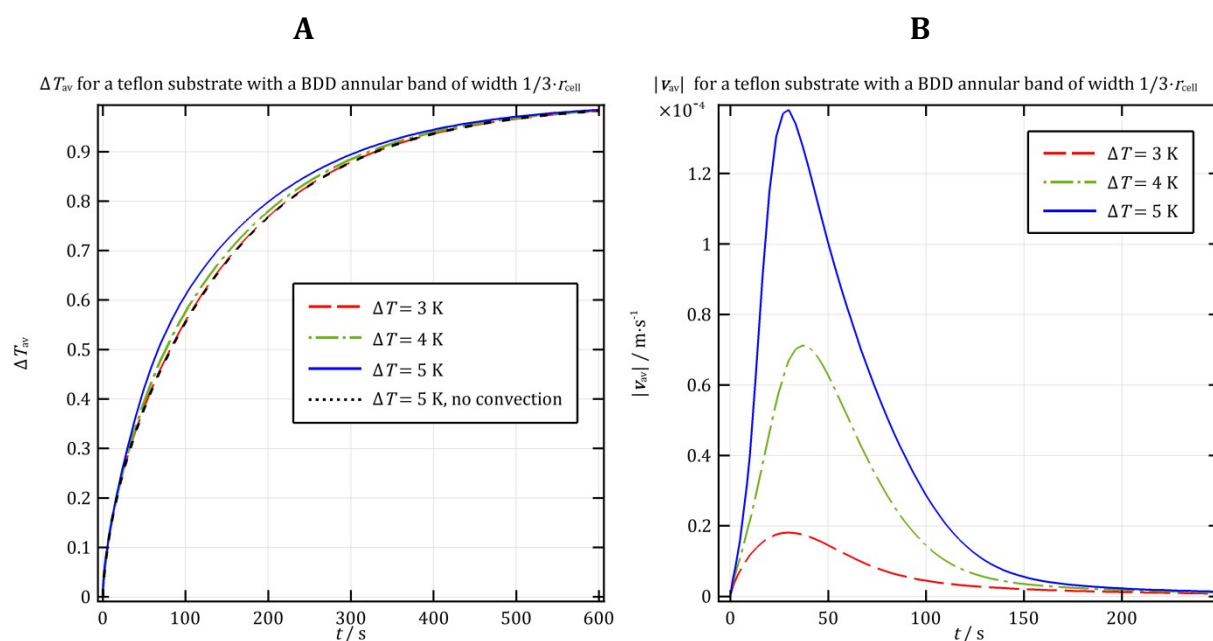


Figure 5. Threshold value of the initial temperature difference ΔT for inducing convective heat transport, illustrated for a teflon substrate with a BDD annular band of width $d_{\text{band}} = 1/3 r_{\text{cell}}$. **A** – volume-averaged temperature difference $\Delta T_{\text{av}}(t)$ – comparison of simulations involving convection with various ΔT and the purely conductive case; **B** – volume-averaged velocity $|v_{\text{av}}(t)|$ plotted for different ΔT .

Lastly, we comment that upon magnification of the velocity distributions discussed both for $r_{\text{cell}} = 3 \text{ mm}$ and below for $r_{\text{cell}} = 8 \text{ mm}$, it is possible to discern small additional vortices, which are situated at $(r_{\text{cell}}, 0)$ and $(r_{\text{cell}}, h_s + h_{\text{cell}})$ and move in the opposite direction to the main one. These vortices may be numerical artefacts or true features of the solution (solutions of this type are seen in Ref. 26), but as they have an intensity that is multiple orders of magnitude lower than the main flow, we do not discuss them in more detail.

1.B. Solution warmer than substrate at $t = 0$ ($\Delta T < 0$)

View Article Online
DOI: 10.1039/C7CP01797A

As it can be expected for a solution that is being cooled from below, for this case heat conduction leads to a stably stratified temperature profile that is not perturbed by the convective flows. Thus, Ra_{cr} is not reached in any of the studied configurations. Nevertheless, as the temperature in the vicinity of inhomogeneous substrates exhibits local variations, non-negligible convective flows arise in cells with substrates of this type, and we describe their most important features below.

Homogeneous substrates

Both for BDD and teflon substrates, the predicted flow in the solution is negligible ($|\mathbf{v}_{max}| \sim 10^{-10}$ - 10^{-9} m·s⁻¹) and does not lead to a significant perturbation of the velocity profile with respect to the conduction-only case, see Figure S18-Figure S21 in the Supplementary Information for details. Furthermore, the velocity profiles obtained from these simulations contain high levels of numerical noise. It is not surprising that only weak convective currents arise for $\Delta T < 0$, since, in this case, the fluid is cooled from below, leading to a local density that is a diminishing function of z , i.e., a stably stratified liquid.

BDD substrates with teflon annular bands

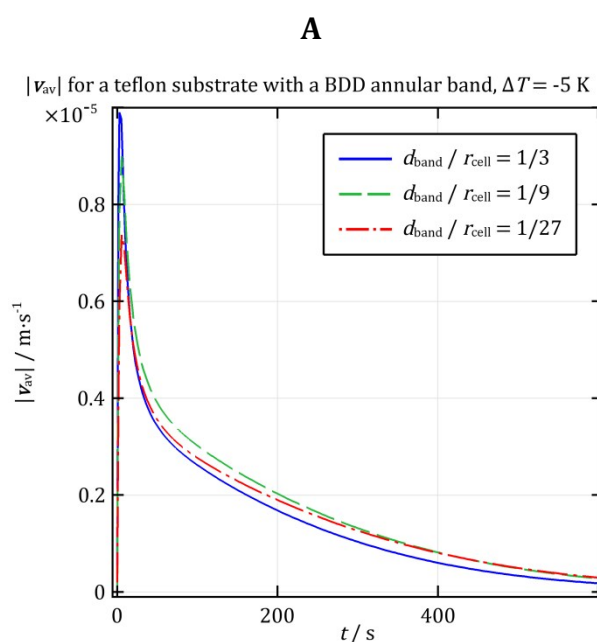
For substrates of this type, the inhomogeneity of the substrate leads to the development of convective currents with an average velocity that strongly depends on d_{band} and is non-negligible for the widest annular band, $d_{band}/r_{cell} = 1/3$ ($|\mathbf{v}_{av}| \sim 10^{-6}$ m·s⁻¹), but the temperature profile in the solution remains unperturbed by the fluid motion (see Figure S23). Interestingly, the flow patterns observed in this configuration are more complicated than for $\Delta T = 5$ K and instead of a single toroidal roll consist of a main roll with a clockwise motion in the simulated region (see Figure 1) that occupies approximately the space between r_1 and r_{cell} along r and between h_s and $h_s + h_{cell}/2$ along z , as well as secondary rolls of lower intensity and direction opposite to that of the main one, see Figure S22. Furthermore, like the case with $\Delta T = 5$ K, the direction of fluid motion in the rolls is relevant to their stability – patterns in which it is reversed with respect to that shown in Figure S22B are unstable - see the Supplementary Information for more details. The direction of flow in the main roll in the stable pattern can be rationalized qualitatively by a similar argument to the one we invoked for inhomogeneous substrates at $\Delta T > 0$. Since the heat conductivity of the teflon annular band is much lower than that of the rest of the substrate, the solution next to it cools down more slowly and rises upwards, leading to the formation of a primary roll with clockwise motion in the primary roll situated between r_1 and r_{cell} .

Teflon substrates with BDD annular bands

For insulating substrates with conductive bands, the average velocity reaches a peak value that is of the order of 10^{-5} m·s⁻¹ for all d_{band} in a characteristic time period of ≈ 5 s

(see Figure 6A) and exhibits slower decay than for $\Delta T = 5$ K (compare with Figure 4A). The pattern of flow here is similar to the one we observed for the 'inverse' configuration, conductive substrates with insulating bands, but with the liquid moving in the opposite direction within the rolls. As Figure 6B shows, there is a main roll with an anticlockwise motion in the simulated region (see Figure 1) occupying approximately the space between r_1 and r_{cell} along r and between h_s and $h_s + h_{\text{cell}}/2$ along z , as well as two secondary ones that possess a much lower intensity and an opposite direction of flow. As we observed for BDD substrates with teflon annular bands, reversing the direction of flow within the rolls leads to an unstable flow pattern, see the Supplementary Information for details. Qualitatively, the temperature of the solution next to the side walls drops more slowly than at the BDD annular band, which makes for an anticlockwise main roll at r between r_1 and r_{cell} .

Despite the comparatively high average velocity within the solution, the temperature within it retains a profile that is indistinguishable from that for heat transfer by conduction only, as demonstrated in Figure 6C and Figure S27.



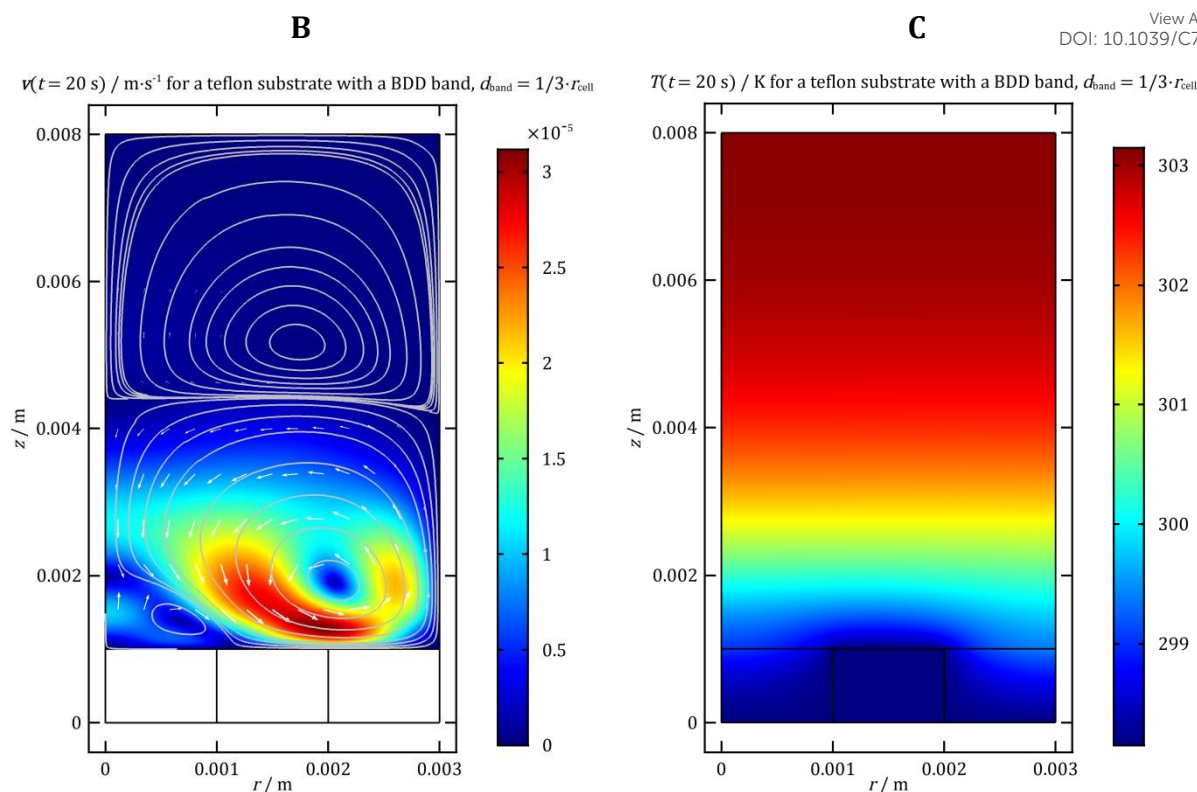


Figure 6. Results for a teflon substrate with a BDD annular band ($d_{\text{band}}/r_{\text{cell}} = 1/3$) and $\Delta T = -5\text{K}$. **A** – volume-averaged velocity magnitude vs. time; **B** and **C** – ‘snapshots’ respectively of v and T at $t = 20\text{ s}$ for a band with $d_{\text{band}}/r_{\text{cell}} = 1/3$. Streamlines in **B** illustrate structure of the flow pattern – the main roll with an anticlockwise movement, at the simulated region for r between r_1 and r_{cell} along r and h and $h_s + h_{\text{cell}}/2$ along z , as well as two secondary rolls – one situated between 0 and r_1 along r and between h_s and $\sim h_s + h_{\text{cell}}/4$ along r and another, possessing the lowest intensity, at the upper half of the cylindrical cell. The length of the arrows in **B** is proportional to natural logarithm of the absolute value of the velocity at the given point. For this simulation, the solution is warmer than the substrate by 5 K at the initial moment.

IV. 2. Simulations for $r_{\text{cell}} = 8\text{ mm}$

We apply the approach of Section IV.1 to the flows within the cell whose radius is chosen so as to guarantee that the volume of liquid in the simulation is approximately equal to that in the experiment. Due to the similarity with the case for a smaller cell, we give fewer details and for substrates with annular bands, we only consider the case $d_{\text{band}}/r_{\text{cell}} = 1/3$. Furthermore, as for this geometry all studied cells are either significantly below or above the critical Rayleigh number, we do not attempt to set bounds for its value.

2. A. Solution colder than substrate at $t = 0$ ($\Delta T > 0$)

BDD substrate

In this case, the natural convective flows reach a peak average velocity of approximately $4 \times 10^{-4}\text{ m}\cdot\text{s}^{-1}$, an order of magnitude higher than for the smaller cell. The change in the aspect ratio of the cylinder exerts a strong effect on the flow patterns, and therefore the velocity distribution. Between $t = 0$ and $t \approx 50\text{ s}$, the flow consists of two rolls lined up in the radial direction and having a width of approximately $r_{\text{cell}}/2$. The two

rolls are comparable in intensity and give rise to a temperature distribution with maxima at $r = 0$ and $r = r_{\text{cell}}$ (see Figure S30). Due to the much stronger convective flow within the solution in comparison with that for the smaller cell, the effect on ΔT_{av} is more pronounced and reaches $\approx 30\%$ at most (Figure S30B). As illustrated in Figure S30, the intensity and shape of these rolls has a complicated evolution, which gives rise to two maxima and two minima in $|\mathbf{v}_{\text{av}}|$. At $t \sim 85$ s, the average solution velocity passes through a third maximum as the two rolls merge into one toroidal roll with anticlockwise motion in the simulated region. The roll in question spans the entire cell, corresponds to the same mode observed in simulations for the smaller cell; the average velocity in the solution tends to zero at $t \approx 400$ s. The transition to a single-roll flow pattern leads to the formation of a temperature distribution with a single maximum at $r = r_{\text{cell}}$.

We should point out that in this case, $|\mathbf{v}_{\text{av}}|$ obtained with quadratic and linear shape functions for T are not completely identical. Such differences in the predicted evolution of the flows arise are to be expected in a system for which the onset of convection is controlled by infinitesimal inhomogeneities in temperature.

We also performed simulations with the boundary condition (29), which permits a non-zero velocity at $t \rightarrow \infty$. The evolution of the velocity and temperature profiles for this case is similar to that illustrated in Figure S30 for a cell with insulated walls and the stationary flow pattern is once again a single toroidal roll. In contrast with what we observed for the smaller cell, the stationary pattern has downward motion in the cylinder centre and a maximum of T at $r = r_{\text{cell}}$, regardless of the choice of shape function order for the temperature. However, if we use a reflection of this flow pattern with respect to $z = h_s$, and a reflection of its corresponding temperature distribution with respect to $r = 0$ as initial conditions (with $p(t = 0) = 0$), we observe that they also correspond to a stationary state. As in the case with the smaller cell, both flows maintain their direction if the boundary condition at the top wall is changed from (29) back to no-flux. Thus, as was seen for $r_{\text{cell}} = 3$ mm, two modes of flow that are equivalent in stability exist in the system.

Teflon substrate

In contrast with our results for the same substrate in the smaller cell, here, we observe significant convective flows that strongly perturb the temperature distribution. As previous studies, e.g. that by Yamaguchi et al.²⁶ show, the critical Ra required to induce the various possible modes of flow in a systems like the presently discussed one is a function of the aspect ratio of the cylinder; thus, it is not surprising that non-negligible flows arise for $r_{\text{cell}} = 8$ mm, but not for $r_{\text{cell}} = 3$ mm.

As with the other cells with a homogeneous substrate at their bottom that exhibit significant convective flows, we observe two modes of flow. The two flow patterns both exhibit a main toroidal roll that occupies most of the cell with either upward or downward motion at $r = 0$, corresponding to a maximum of T at $r = 0$ or $r = r_{\text{cell}}$,

respectively. In both cases, the flow contains an additional roll with direction opposite to the main flow; the size and intensity of the latter diminish over time. For the pattern with positive normal velocity at $r = 0$, this roll is situated at the vicinity of the point (r_{cell}, h_s) and leads to an additional perturbation in the temperature profile, which is eventually smoothed out (see Figure S31C-F in the Supplementary Information). For the other pattern, the smaller roll is situated approximately at $(r_{\text{cell}}, h_s + h_{\text{cell}})$ and does not perturb the velocity distribution.

Similarly to the case of a BDD substrate at $r_{\text{cell}} = 3$ mm, the two flow patterns that differ by the sign of v_z at $r = 0$ can be obtained by varying the order of the shape functions for T . Applying the same methodology used for the stability analysis of flows generated in cells with homogeneous BDD substrates at $r_{\text{cell}} = 3$ mm leads to the conclusion that, once again, the two observed modes of flow are equivalent in stability.

The average solution velocity passes through several extrema, reaching a global maximum value of 3.2 and $4.1 \times 10^{-4} \text{ m} \cdot \text{s}^{-1}$ for the pattern with upflow and downflow at $r = 0$, respectively. The effect of convection on ΔT_{av} , while substantial, is not as strong as in the analogous system with a conductive substrate and reaches at most 10 and 14% for the flows with upwelling and downward motion at $r = 0$. Plots of $|\mathbf{v}_{\text{av}}|$, ΔT_{av} , as well as 'snapshots' of the velocity and temperature distributions can be found in the Supplementary Information (Figure S31- Figure S32).

BDD substrate with a teflon annular band

The convective flows generated in this case evolve through multiple stages; the volume-averaged solution velocity reaches a peak value of $4.5 \times 10^{-4} \text{ m} \cdot \text{s}^{-1}$, an approximately five-fold increase with respect to the result for the smaller cell – compare Figure 3A and Figure 7A. The heat transfer in the liquid is strongly affected, and the difference in ΔT_{av} induced by convection peaks at 44%, see Figure 7B.

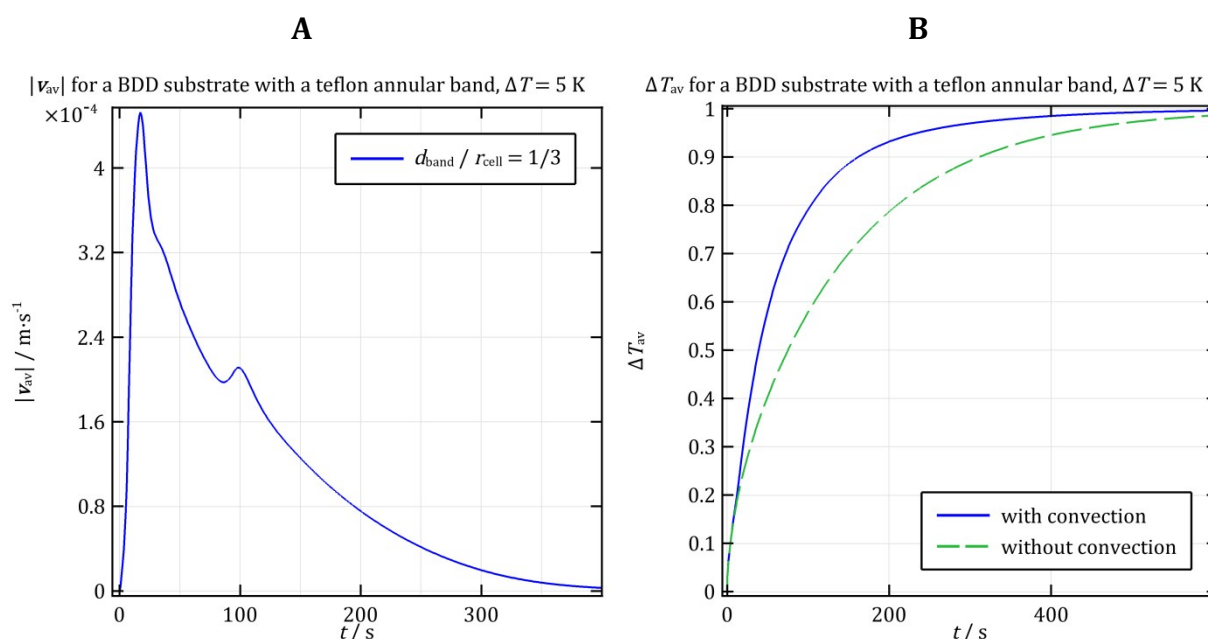


Figure 7. Results for a BDD substrate with a teflon annular band situated at the bottom of a cell of radius 8 mm. The solution is initially colder than the substrate ($\Delta T = 5$ K). **A** – $|v_{av}|$ vs. t ; **B** – volume averaged dimensionless ΔT_{av} vs. t .

As observed for a homogeneous BDD substrate, the flow initially consists of two counter-rotating rolls stacked in the radial direction that give rise to a temperature distribution with maxima at $r = 0$ and $r = r_{cell}$, as illustrated in Figure 8A-B. Notably, the intense heat flux coming through the BDD surface causes the fluid in contact with it to rise upwards, leading to the formation of a two rolls, the more intense of which is situated at $r \lesssim r_{cell}/2$ along r and has clockwise motion in the simulated region. Another similarity with the case of a BDD substrate is that as time progresses, the two rolls merge into one that occupies the whole cylinder and has upwelling next to the walls (Figure 8C). As a consequence of that, the temperature distribution adopts a shape with a single maximum at $r = r_{cell}$ (Figure 8D).

Qualitative stability analysis of the flow patterns in this system, explained in more detail in the Supplementary Information, shows that the single roll with upward motion next to the walls is stable and that its mirror image with respect to $z = h_s$ is unstable. This is analogous to our result for a substrate of the same type situated at the bottom of a smaller cell.

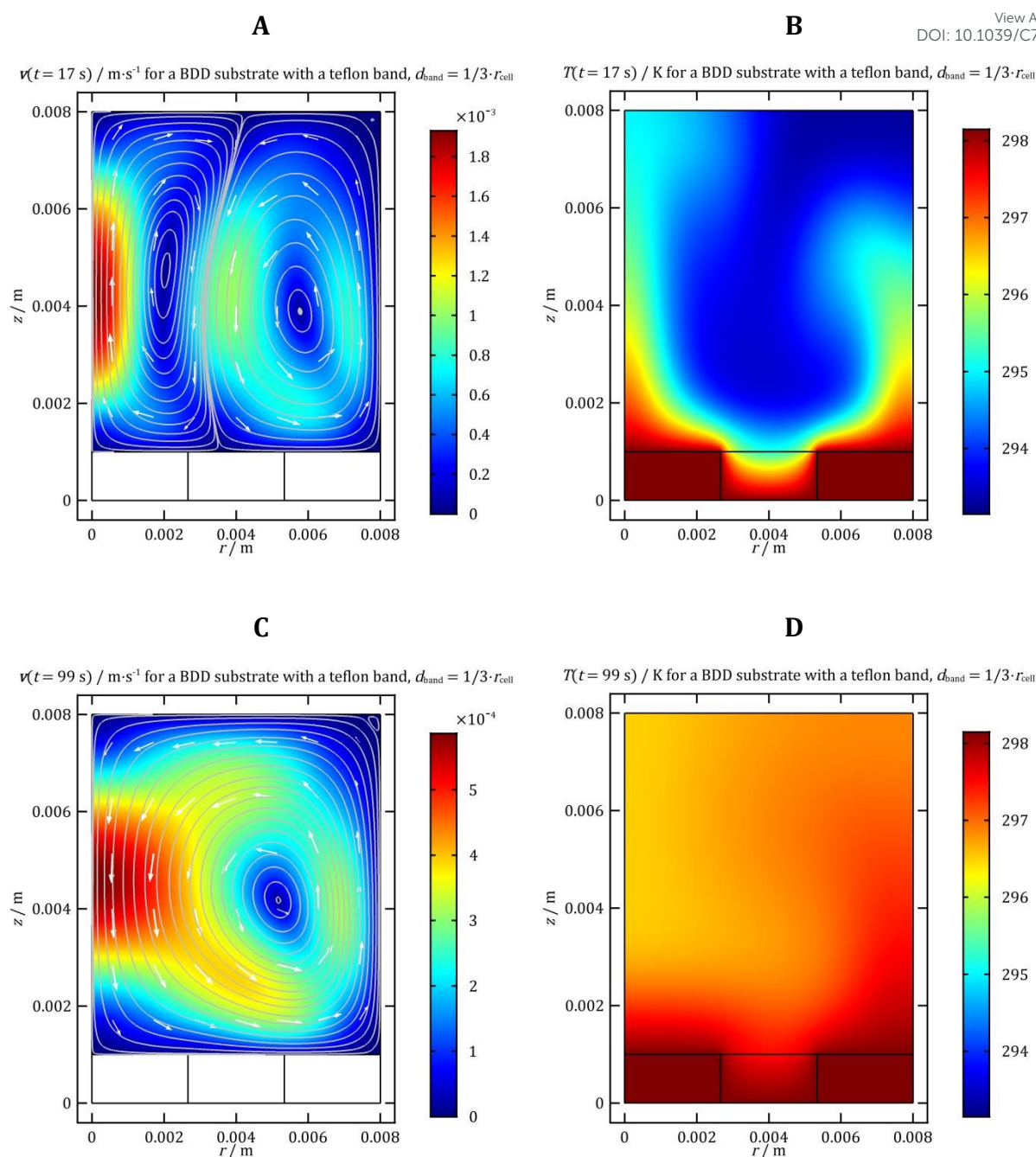


Figure 8. Profiles of v and T for a BDD substrate with a teflon band ($d_{\text{band}}/r_{\text{cell}} = 1/3$). The ‘snapshots’ of the velocity and temperature distributions in **A–D** are taken at the two maxima of $|v_{\text{av}}|$, $t = 17 \text{ s}$ and $t = 99 \text{ s}$. **A** illustrates the velocity distribution with streamlines illustrating the two transient convective rolls; **B** – the temperature distribution that this flow pattern brings about. **C** shows the single-roll velocity pattern that results from the merging of the two rolls in **A**; **D** demonstrates the profile of T corresponding to it. The length of the arrows in **A** and **C** is proportional to natural logarithm of the absolute value of the velocity at the given point. For this simulation, the solution is colder than the substrate at $t = 0$ ($\Delta T = 5 \text{ K}$).

Teflon substrate with a BDD annular band

This configuration gives rise to convective flows that have a peak average velocity of $5 \times 10^{-4} \text{ m} \cdot \text{s}^{-1}$, a nearly five-fold increase with respect to the case of a smaller cell (see Figure S33A). Furthermore, the effect of convection on the temperature distribution is

much more substantial, amounting to a 39 % difference in ΔT_{av} at most, as illustrated in Figure S33B in the Supplementary Information.

As in the 'inverse' configuration, the flow initially consists in two counter-rotating rolls, which perturb the temperature profile strongly and induce a maximum in T at $r \sim r_1$. Again, the fluid motion is most intense and directed upwards in the vicinity of the BDD due to the local increase in temperature there, causing a roll with clockwise motion in the simulated region to appear at $r \gtrsim r_{cell}/2$. At longer times, the two convective cells merge to form a single toroidal roll that occupies the whole cylinder and has upwelling at $r = 0$; the temperature profile corresponding to it has a warmer region at $r = 0$. The evolution of the distributions of T and \mathbf{v} is illustrated in Figure S33C-F in the Supplementary Information.

By applying the same qualitative stability analysis we used in our analysis of substrates of the same type at $r_{cell} = 3$ mm, we see that in this case, as we observed for $r_{cell} = 3$ mm, the roll in which the fluid moves downward instead of upward at $r = 0$ is unstable.

2. B. Solution warmer than substrate at $t = 0$ ($\Delta T < 0$)

Homogeneous substrates

As in the smaller cell, due to the stable stratification of the fluid, no significant convective flows arise within the system if it contains a homogeneous substrate that is colder than the solution at $t = 0$. For both BDD and teflon substrates, the simulations yield negligible fluid motion ($|\mathbf{v}_{av}| \sim 10^{-9}$ m·s⁻¹), which does not influence the temperature profile.

BDD substrate with a teflon annular band

In this system, the inhomogeneity of the substrate generates local density variations in the liquid and convective flows, but the intensity of the latter is greater by an order of magnitude than it is for the smaller cell ($|\mathbf{v}_{av}| \sim 10^{-5}$ vs. 10^{-6} m·s⁻¹). Despite the considerable velocity of the fluid, the temperature profiles remain unaffected by convection, as they do for the smaller cell. The flow undergoes complex evolution but passes through a three-roll configuration similar to that observed for the small cell – a main roll with clockwise movement in the simulated region (see Figure 1) situated approximately between $r_1 + d_{band}/2$ and r_{cell} along r and h_s and $h_s + h_{cell}/2$ along z , as well as two secondary rolls of opposing direction and lower intensity. Plots of $|\mathbf{v}_{av}|$, ΔT_{av} and 'snapshots' of the velocity and temperature distributions can be found in the Supplementary Information (Figure S34).

The flow pattern in this system was subjected to the same stability tests described for the smaller cell. Once again, the tests indicate that the direction of flow within the rolls is determined by the substrate structure and that reversing it leads to an unstable

flow pattern. Though there are differences between the velocity profiles observed for $r_{\text{cell}} = 3$ and 8 mm, the qualitative explanation for the flow direction in the main roll is the same – the fluid next to the annular band is cooled down at a slower rate than that in contact with the rest of the substrate, which leads to a circulatory pattern for r between r_1 and r_{cell} that moves clockwise in the simulated region of space (see Figure 1).

Teflon substrate with a BDD annular band

As with the ‘inverse’ configuration, significant convective flows arise in this system and their intensity is increased with respect to the simulations for the smaller cell ($|\mathbf{v}_{\text{av}}|_{\text{max}} \sim 4 \times 10^{-5}$ vs. $0.9 \times 10^{-5} \text{ m}\cdot\text{s}^{-1}$). As in the other systems with a substrate that is initially colder than the solution, the temperature profile in the liquid remains unaffected by convection in spite of the non-negligible flows. The velocity profile has a complicated evolution, but passes through a configuration with three rolls, as for a BDD substrate with a teflon annular band. Importantly, as we observed in the case with $r_{\text{cell}} = 3$ mm, the direction of flow within the rolls is opposite to that for substrates with the ‘inverse’ structure.

The direction of movement in the rolls has the same qualitative explanation we invoked in the discussion of the results for the smaller cell. Due to the lower heat conductivity of the teflon, the fluid in contact with the outer ring between $r_1 + d_{\text{band}}$ and r_{cell} remains warmer than that in touch with the boron-doped diamond and rises upward, thus giving rise to a main roll in which the liquid in the simulated region (Figure 1) moves anticlockwise.

The analysis of the stability of this flow pattern, performed in a completely analogous way to the one we did for the smaller cell, indicates that the direction of flow in the cells is once again determined by the profile of the heat conductivity within the solid substrate and that a flow in which the sense of the rolls is reversed is unstable.

The Supplementary Information contains additional data on this system in the form of plots of $|\mathbf{v}_{\text{av}}|$, ΔT_{av} and ‘snapshots’ of the velocity and temperature distributions (see Figure S35).

Non-aqueous solvents

Our study deals specifically with aqueous solutions as this is the medium used for the vast majority of electrochemical and SECM experiments, but it would be straightforward to apply the approach described in our paper to other solvents. Naturally, using a more viscous solvent – for example, dimethyl sulfoxide, whose viscosity is higher than that of water by a factor of two³³ – would lead to less pronounced natural convective currents. Conversely, using a less viscous solvent, such as N,N-dimethylformamide ($\eta(T = 298.15 \text{ K}) = 0.794 \text{ mPa}\cdot\text{s}$ ¹⁴) would make natural convection even more pronounced. However, the precise behaviour of the liquid would be determined by the corresponding values of Pr and Ra . Taking the example of DMF

and the following values for its material properties at 298.15 K: $\alpha_{\text{DMF}} = 1.013 \times 10^{-3} \text{ K}^{-1}$ from Ref. 34, $\kappa_{\text{DMF}} = 0.183 \text{ W} \cdot \text{m}^{-1} \cdot \text{K}^{-1}$ and $\rho_{\text{DMF}} = 944.5 \text{ kg/m}^3$ and $C_{p\text{DMF}} = 2.06 \times 10^3 \text{ J} \cdot \text{kg}^{-1} \cdot \text{K}^{-1}$ from Ref. 14, we can compare the values of Ra and Pr with those for water at 293.15, obtaining $Pr_{\text{DMF}}/Pr_{\text{H}_2\text{O}} = 1.3$ and $Ra_{\text{DMF}}/Ra_{\text{H}_2\text{O}} = 8.9$, the latter indicating that flows in DMF would be considerably more susceptible to natural convection driven by thermal gradients. However, it is worth mentioning that changing the solvent would also affect the mass transport in the system through the temperature dependence of the viscosity, and therefore the diffusion coefficients of the species present in solution.

V. Conclusions

This paper presents a numerical study of the convective heat transfer in an idealized model of an electrochemical measurement cell consisting of a solid substrate with a thermostated lower surface situated at the bottom of a cylindrical cell with solid, thermally insulated walls. We have shown that under the conditions prescribed in the model, the substrate structure, or, more precisely, the spatial distribution of thermal conductivity, plays an important role in the evolution of the temperature and velocity profiles. The simulations described here demonstrate that an initial temperature difference between the solution and the substrate may generate flows which evolve over a time scale of $\sim 100 \text{ s}$ and have average velocities as high in order in magnitude as $10^{-4} \text{ m} \cdot \text{s}^{-1}$. Such flows can strongly perturb the temperature profile within the solution and presumably also influence mass transport. Moreover, we have shown that the intensity and direction of these flows may vary depending on the initial temperature difference and on the spatial distribution of thermal conductivity within the substrate.

As discussed in Section IV.1, for homogeneous substrates in the cell of radius 3 mm, appreciable natural convective flows (of $|\mathbf{v}_{\text{av}}| \sim 10^{-5} \text{ m} \cdot \text{s}^{-1}$) only arise if the liquid is initially colder than the substrate and the latter is thermally conductive. We have also demonstrated that convective flows of non-negligible intensity (of $|\mathbf{v}_{\text{av}}| \sim 10^{-6} \text{--} 10^{-5} \text{ m} \cdot \text{s}^{-1}$) arise in the case of inhomogeneous substrates with an annular band, and that the width of the band in question influences the velocity magnitude in the fluid (see Figure 3A, Figure 4A and Figure 6A). This is true regardless of the sign of the initial temperature difference between solution and substrate, even though convection only leads to a strong perturbation of the temperature if the solution is colder than the substrate at the initial moment (compare Figure 5, Figure S9 and Figure S14 with Figure S23 and Figure S27). In addition to that, analysis of the stability of the natural convective flows arising in all systems with inhomogeneous substrates regardless of the sign of ΔT indicates that the direction of fluid movement within the stable flow pattern is determined by the structure of the substrate.

For the larger cell, provided that the solution is initially colder than the solid substrate ($\Delta T > 0$), significant convective flows arise regardless of the conductivity of the latter. In the case of a conductive substrate, the volume-averaged velocity reaches a

maximum value of the order of $10^{-4} \text{ m}\cdot\text{s}^{-1}$, an increase of one order of magnitude in comparison with the result for the smaller cell. A similar increase is observed in the effect of convection on ΔT_{av} – for the large container, reaches as much as 40% instead of several percent. Furthermore, we have observed that at $r_{\text{cell}} = 8 \text{ mm}$, the velocity and temperature profiles undergo a much more complex evolution (compare Figure 2 and Figure S30). For $\Delta T > 0$, the velocity and the effect on ΔT_{av} see an approximately tenfold increase for systems containing substrates with annular bands (compare Figure 7- Figure 8 with Figure 3 and Figure S33 with Figure 4). Both for conducting and insulating bands, at long times the velocity profiles consist of a single toroidal roll occupying the whole cylinder. For the case of $\Delta T < 0$, for which the solution is warmer than the substrate at $t = 0$, we observe no qualitative difference between the two studied cells – for the larger cell, significant convective flows ($|\mathbf{v}_{\text{av}}| \sim 10^{-5} \text{ m}\cdot\text{s}^{-1}$) arise only for substrates with inhomogeneous thermal conductivity. While the velocity magnitude is increased by up to an order of magnitude with respect to the case with $r_{\text{cell}} = 3 \text{ mm}$, the temperature distribution remains unperturbed by convection (compare Figure S34 with Figure S22 and Figure S35 with Figure 6). As we observed for the smaller cell, the direction of the flow in the stable flow patterns in systems with inhomogeneous substrates is determined by the substrate structure.

Our results for the velocity distribution, although pertaining to a highly idealized system, highlight the importance substrate structure can have on electrochemical experiments performed with thermostating through the said substrate unless it is ensured that the system has reached thermal equilibrium before any measurements are performed. As we noted in the Introduction and our previous work dealing with imperfect thermostating³, the observed natural convective flows have the potential to seriously compromise data from such electrochemical experiments. In particular, our results indicate that conclusions drawn from non-thermostated SECM measurements of heterogeneous surfaces such as basal/edge plane graphite need to be treated with caution, especially where they deviate from inferences made under more rigorous conditions. This caveat applies in equal measure to stationary and transient SECM measurements.

On a more general note, as the simulations of two different cells discussed here show, even in a highly simplified system there are multiple factors that can influence the intensity and structure of the flows generated by imperfect thermostating, and the precise geometry of the container is of particular importance. Thus, attempting to take natural convection into account in experimental setups where thermal convection is likely to arise would be impractical. Moreover, results obtained in the presence of natural convective flows would not be reproducible between containers that differ in shape. These difficulties could be avoided by ensuring that the solution temperature is homogeneous during the measurements, which would render the contribution of thermal convection to mass transport negligible.

Acknowledgements. We are indebted to Prof. Ian Hewitt, Prof. Philip Maini and Dr. Thomas Woolley, all of them from the Mathematical Institute of the University of Oxford, for very helpful discussions and valuable suggestions. J.K.N. thanks the Clarendon Fund and Trinity College of the University of Oxford for financial support.

References

1. J.K. Novev, S. Eloul and R.G. Compton, *J. Phys. Chem. C*, 2016, **120**, 13549.
2. K. Ngamchuea, S. Eloul, K. Tschulik and R.G. Compton, *Anal. Chem.*, 2015, **87**, 7226.
3. J.K. Novev and R.G. Compton, *Phys. Chem. Chem. Phys.*, 2016, **18**, 29836.
4. D.T. Sawyer, A. Sobkowiak and J.L. Roberts, *Electrochemistry for Chemists*, Wiley, New York, 1995.
5. A.J. Bard, F.-R.F. Fan, J. Kwak and O. Lev, *Anal. Chem.*, 1989, **61**, 132.
6. J. Kwak and A.J. Bard, *Anal. Chem.*, 1989, **61**, 1794.
7. M.V. Mirkin, W. Nogala and J. Velmurugan, Y. Wang, *Phys. Chem. Chem. Phys.*, 2011, **13**, 21196.
8. D. Schäfer, A. Puschhof and W. Schuhmann, *Phys. Chem. Chem. Phys.*, 2013, **15**, 5215.
9. K.B. Holt, A.J. Bard, Y. Show and G.M. Swain, *J. Phys. Chem. B*, 2004, **108**, 15117.
10. R.J. Bowling, R.T. Packard and R.L. McCreery, *J. Am. Chem. Soc.*, 1989, **111**, 1217.
11. R.L. McCreery, *Chem. Rev.*, 2008, **108**, 2646.
12. R.L. McCreery, A. Bergren, A. Morteza-Najarian, S.Y. Sayed and H. Yan, *Faraday Discuss.*, 2014, **172**, 9.
13. G. A. Slack, *Phys. Rev.* 1962, **127**, 694.
14. D.R. Lide, Ed., *CRC Handbook of Chemistry and Physics, Internet Version 2005*, CRC Press, Boca Raton, FL, 2005.
15. P. Bergé and M. Dubois, *Contemp. Phys.*, 1984, **25**, 535.
16. R. Touihri, H. Ben Hadid and D. Henry, *Phys. Fluids*, 1999, **11**, 2078.
17. D.A. Kaminsky and C. Prakash, *Int. J. Heat Mass Transfer*, 1986, **29**, 1979.
18. N.H. Saeid, *Int. J. Therm. Sci.*, 2007, **46**, 531.
19. D.M. Kim, R. Viskanta, *J. Heat Transfer*, 1985, **107**, 139.
20. R. B. Bird, W.E. Stewart and E.N. Lightfoot, *Transport Phenomena*, 2nd Edition, Wiley, New York, NY, 2002.
21. P. K. Kundu and I. M. Cohen, *Fluid Mechanics*, 2nd Edition, Academic Press, San Diego, CA, 2002.
22. A.J. Bard, M.V. Mirkin (Eds.), *Scanning Electrochemical Microscopy*, 2nd Edition, CRC Press, Boca Raton, 2012.

23. E.J.F. Dickinson, H. Ekström and E. Fontes, *Electrochem. Commun.*, 2014, **40**, 71. View Article Online
DOI: 10.1039/C4CP01797A
24. G. Neumann, *J. Fluid Mech.*, 1990, **214**, 559.
25. K.E. Torrance, L. Orloff and J.A. Rockett, *J. Fluid Mech.*, 1969, **36**, 21.
26. Y. Yamaguchi, C.J. Chang and R.A. Brown, *Phil. Trans. R. Soc. Lond. A*, 1984, **312**, 519.
27. D. Prikhodko, S. Tarelkin, V. Bormashov, A. Golovanov, M. Kuznetsov, D. Teteruk, A. Volkov, S. Buga, *MRS Commun.*, 2016, **6**, 71.
28. C.A. Harper, Ed., *Modern Plastics Handbook*, McGraw-Hill, New York, NY, 1999.
29. J. Blumm, A. Lindemann, M. Meyer and C. Strasser, *Int. J. Thermophys.*, 2010, **31**, 1919.
30. D.M. Price and M. Jarratt, *Thermochim. Acta*, 2002, **231**, 392-393.
31. S.F. Lau, H. Suzuki and B. Wunderlich, *J. Polym. Sci. Polym. Phys. Ed.*, 1984, **22**, 379.
32. G. Müller, G. Neumann and W. Weber, *J. Cryst. Growth*, 1984, **70**, 78.
33. J.N. Butler, *J. Electroanal. Chem.*, 1967, **14**, 89.
34. G.I. Egorov, A.M. Kolker, *Russ. J. Phys. Chem. A*, 2008, **82**, 2058.